Published in final edited form as:
J Neurochem. 2012 June ; 121(6): 852–860. doi:10.1111/j.1471-4159.2012.07743.x.

Spatially restricted actin-regulatory signaling contributes to synapse morphology

Daniel A. Nicholson, Ph.D.[*,1], **Michael E. Cahill, Ph.D.**[†,1], **Christopher T. Tulisiak, B.S.**[*], **Yuri Geinisman, M.D., Ph.D.**[‡], and **Peter Penzes, Ph.D.**[†,§]

[*]Department of Neurological Sciences, Rush University Medical Center, Chicago, IL 60612.

[†]Department of Physiology, Northwestern University Feinberg School of Medicine, Chicago, IL 60611.

[‡]Department of Cell and Molecular Biology, Northwestern University Feinberg School of Medicine, Chicago, IL 60611.

[§]Department of Psychiatry and Behavioral Sciences, Northwestern University Feinberg School of Medicine, Chicago, IL 60611.

Abstract

The actin cytoskeleton in dendritic spines is organized into microdomains, but how signaling molecules that regulate actin are spatially governed is incompletely understood. Here we examine how the localization of the RacGEF kalirin-7, a well-characterized regulator of actin in spines, varies as a function of postsynaptic density (PSD) area and spine volume. Using serial section electron microscopy (EM), we find that extrasynaptic, but not synaptic, expression of kalirin-7 varies directly with synapse size and spine volume. Moreover, we find that overall expression levels of kalirin-7 differ in spines bearing perforated and non-perforated synapses, due primarily to extrasynaptic pools of kalirin-7 expression in the former. Overall, our findings indicate that kalirin-7 is differentially compartmentalized in spines as a function of both synapse morphology and spine size.

Introduction

Dendritic spines are the sites of most excitatory synaptic connections in the central nervous system. Spine number and morphology change in adult plasticity (Alvarez & Sabatini 2007; Yuste 2011), and spine morphology and density undergo changes in live animals in several behavioral conditions such as learning (Comery *et al.* 1996), during social interactions (Silva-Gomez *et al.* 2003), and as a result of aging (Nicholson *et al.* 2004). Moreover, alterations in synaptic structure and function are associated with neuropsychiatric disorders (Penzes *et al.* 2011; Glantz & Lewis 2000).

Recent studies have shown that the actin cytoskeleton of dendritic spines is organized in functional subdomains, and that polymerized actin is highly concentrated in spine areas outside of the postsynaptic density (PSD) (Frost *et al.* 2010b; Honkura *et al.* 2008). Such tight spatial control within the ~ 1 um^3 volume of the spine would require equally spatially-restricted signaling cascades that control actin dynamics. It is unclear how molecules that relay signals from surface receptors in the PSD to actin-binding proteins are spatially

Correspondence should be addressed to Peter Penzes, 303 E. Chicago Ave, Chicago, IL 60611; p-penzes@northwestern.edu Phone 312-503-5379; Fax 312-503-5101..
[1]These authors contributed equally

regulated within individual spines. As many signaling molecules in spines, such as RacGEFs, are associated with the PSD, it is possible that receptor-induced signaling events occur largely at or near the PSD. In this case, the spatial control of the actin subdomains could be achieved primarily by the spatial localization of molecules that directly bind and modify actin (Frost *et al.* 2010a). However, another alternative is that signaling molecules known to be enriched in the PSD might be spatially regulated in multiple spine microdomains.

To distinguish between these possibilities, we used serial section, postembedding immunogold electron microscopy (immuno-EM) to examine how the localization of a well-characterized actin regulator in spines, the RacGEF kalirin-7 (Penzes & Jones 2008), varies as a function of synapse size, morphology, and spine volume. Kalirin is a brain-specific GEF for Rho-like small GTPases (Penzes *et al.* 2008; Penzes & Jones 2008), with expression restricted mainly to the cerebral cortex and hippocampus (Ma *et al.* 2001). Kalirin-7 is the most abundant postnatally expressed kalirin isoform, and is a major regulator of forebrain spine morphogenesis: its overexpression increases spine size, while kalirin knockdown reduces spine area (Penzes *et al.* 2000; Penzes *et al.* 2001a; Xie *et al.* 2007). In addition to the regulation of basal spine maturation and maintenance, kalirin-7 is important for activity-dependent changes in spine structure and function (Xie et al. 2007), and mediates signaling by synaptic receptors including NMDA receptors, EphB, erbB4, and $5HT_{2A}$ (Xie et al. 2007; Penzes & Jones 2008; Jones *et al.* 2009; Cahill *et al.* 2012). The C-terminus of kalirin-7 interacts with PDZ domain-containing proteins (Penzes *et al.* 2001b); however, how kalirin-7's localization within spines relates to synapse morphology and spine size remains unknown.

Materials and Methods

Antibodies and Reagents

Monoclonal anti-PSD-95 antibody was purchased from Neuromab. Polyclonal antibody against kalirin-7 has been previously described (Penzes et al. 2000).

Immunogold electron microscopy

For post-embedding immunogold electron microscopy, three young adult rats (3-6 months) were fixed via intra-cardial perfusion with 100 ml of 0.12M phosphate buffer, followed by 1000 ml of ice-cold 4% paraformaldehyde/0.5% glutaraldehyde in 0.12M phosphate buffer. The brain was then removed, hemisected, and postfixed for 2 hours. Brains were rinsed, and slices were obtained with a tissue chopper at 300 μm thickness. These slivers were then cryoprotected in escalating concentrations of glycerol, and plunge frozen in liquid propane using a Leica EM CPC. Slivers were then transferred into a Leica AFS freeze-substitution device, treated with 1.5% uranyl acetate in methanol at −90°C, infiltrated with Lowicryl HM20 resin (Electron Microscopy Sciences, Fort Washington, PA) at −45°C, and polymerized with ultraviolet light. Slivers were trimmed to obtain ultrathin sections that included the entire somatodendritic extent of the CA1 stratum radiatum. Ribbons of consecutive serial sections (>30 sections per series) were mounted on pioloform-coated nickel slot grids. On-grid staining began with first immersing grids in a saturated solution of NaOH in absolute ethanol for 2-3 seconds, rinsing in distilled water, and incubating in 0.1% sodium borohydride and 50 mM glycine in 5 mM Tris buffer (pH 7.4), containing 0.05% Triton X-100 and 0.8% NaCl (TBST) for 10 minutes. Treatment with 10% normal goat serum (NGS) in TBST (pH 7.4) for 30 minutes was followed by incubation in rabbit purified anti-kalirin-7 primary antibody overnight at 4°C at a concentration of 1:100, diluted in TBST (pH 7.4) containing 1% NGS. After a thorough rinse in TBST, sections were blocked in 1% NGS in TBST (pH 8.2) for 20 minutes and then incubated for 1 hour in secondary

antibodies conjugated with 10-nm gold particles (GAR10; British BioCell International, Cardiff,United Kingdom). The secondary antibodies were diluted 1:20 in TBST (pH 8.2) containing 1% NGS and 0.5% polyethylene glycol. Finally, sections were thoroughly rinsed in TBST, followed by distilled water, and then stained with uranyl acetate and lead citrate.

Serial section electron micrographs were obtained using a JEOL 100CX transmission electron microscope. Synapses were identified on the electron micrographs and characterized as either perforated or non-perforated, based on the presence or absence of a discontinuity in their PSD in at least one sectional profile, respectively. PSD area was estimated as the product of the length of the PSD (excluding the electron-lucent perforation in perforated PSDs) and section thickness (67 nm, determined using Small's method of minimal folds). The immunogold synaptic analyses derive from a total of 500 non-perforated synapses and 172 perforated synapses. The immunogold spine volume analyses are based on 102 complete spines, traceable back to their parent dendrite, of which 24 bore a perforated synapse and 78 bore a non-perforated synapse. Spine volume was estimated as the product of the total spine area and section thickness. All micrographs were obtained from the middle portion of CA1 stratum radiatum.

Electron micrograph films were scanned and digitized using an Epson 10000XL scanner, aligned into stacks of serial sections, and optimized for visualization by adjusting the gray levels in Adobe Photoshop (Adobe Systems, Inc., San Jose, CA). All analyses were performed on these gray level-adjusted stacks. PSD measurements were performed as described previously (Nicholson *et al.* 2006; Nicholson & Geinisman 2009). Briefly, the length of each PSD segment was measured in serial sections for each synapse in NIH Image, and then corrected for magnification (28,000X) and converted into microns. Spine volume measurements were obtained on these same digitized micrographs.

Immunogold particles were considered synaptic if they were projected onto the PSD, within the synaptic cleft, or otherwise within 20nm of the PSD. Extrasynaptic particles for the analysis in figures 2 and 3 were those particles within the spine head, between 20nm and 150nm of the PSD on a single section, while perisynaptic particles for the analysis in figure 4 were particles within a window that corresponds to the approximate depth of a typical PSD (20-60nm from the PSD). Spinous particles in figure 4 were all other immunogold particles within the spine head or neck. Background staining was very low, as indicated by the absence of immunogold particles on mitochondria and the near absence of labeling in the axon terminals.

Immunofluorescence

To measure the intensity of kalirin-7 immunostaining as a function of endogenous PSD-95 area, images were acquired a Ziess LSM5 Pascal confocal microscope. Images of neurons were taken using a 63× oil-immersion objective as a z-series of three to eight images, averaged four times, taken at 0.37μm intervals, 1024 × 1024 pixel resolution. The background corresponding to areas without cells was subtracted to generate a "background-subtracted" image. To measure the intensity of kalirin-7 clusters localized within PSD-95 puncta, regions defining PSD-95 puncta were generated based on fluorescence in one channel. These regions were then transferred to the kalirin-7 fluorescence channel, and only the kalirin-7 fluorescence intensities within the corresponding PSD-95 puncta were measured; the kalirin-7 images were thresholded equally. In order to prevent saturation of the kalirin-7 signal during imaging, the detection gain was altered for each neuron, and the relationship between PSD-95 area and endogenous kalirin-7 integrated intensity was analyzed independently for each neuron. Data were then normalized across all cells. To do this, for each cell the integrated kalirin-7 intensity or density of individual puncta was

divided by the average of all kalirin-7 puncta integrated intensity for that cell. Fluorescent intensities were quantified using MetaMorph (Universal Imaging Corporation).

Statistics

Statistics used for multiple group analyses are provided in the figure legends. Statistical analyses for two group comparisons were done with Student's t-test. For multiple comparisons, an ANOVA was used with a Bonferroni or Tukey post-hoc test. The relationship between PSD area and the amount of synaptic or extrasynaptic kalirin-7, and the relationships between spine volume and kalirin-7 particle numbers in various spine microdomains were determined using linear regression analysis. Differences were deemed statistically significant when $p<0.05$. Data were analyzed using GraphPad Prism (La Jolla, CA, USA).

Results

We first immunostained cortical neurons for endogenous PSD-95 and kalirin-7. As PSD-95 is among the most prominent molecules in the post-synaptic density (Newpher & Ehlers 2009), its label allows for the visualization of a spine's synaptic region. We determined the integrated density (area x mean fluorescent intensity) and the integrated intensity (sum of fluorescent intensity for a given area) of individual endogenous kalirin-7 puncta along dendrites as a function of the corresponding PSD-95 puncta area (Fig. 1a). We found a positive and significant correlation between PSD-95 puncta area and kalirin-7 integrated density ($r^2=0.854$; best fit slope=5.48±0.07; $p<0.0001$; Fig. 1b) and integrated intensity ($r^2=0.544$; best fit slope=5.50±0.15; $p<0.0001$; Fig. 1c). The linear relationship between PSD-95 area and total kalirin-7 content was further confirmed by examining kalirin-7 integrated intensity as a function of PSD-95 binned area (Fig. 1d). Collectively, this suggests that the amount of kalirin-7 in the spine head increases as a linear function of increased PSD area.

We were interested in determining whether this increase in kalirin-7 arose from its synaptic or extrasynaptic localization. Owing to its limited point spread function, confocal microscopy does not allow for the delineation between synaptic and extrasynaptic spine compartments, and the increase in kalirin-7 intensity with increasing PSD-95 puncta area could arise from synaptic domains, extrasynaptic domains, or both. To determine if kalirin-7's subspine localization varies as a function of PSD area, we used serial section postembedding immunogold electron microscopy (immunoEM) to examine the localization of kalirin-7 in spines and their synapses across a broad range of morphologies. Reconstructions of spines are shown in Fig. 2a-c. Spines and their synapses could be immunopositive for kalirin-7 in both synaptic and extrasynaptic domains (Fig. 2a), only extrasynaptically (Fig. 2b) or only synaptically (Fig. 2c). As found in cultured cells, we found that the total kalirin-7 content of spines increased linearly with PSD area. We found a significant correlation between PSD area and the amount of extrasynaptic kalirin-7 ($r^2=0.237$; best fit slope=41.21±2.86; $p<0.0001$; Fig. 2d). We also found a significant correlation between PSD area and the amount of synaptic kalirin-7; however, the correlation between these two parameters was minimal ($r^2=0.036$; best fit slope=8.31±1.65; $p<0.0001$; Fig. 2e). Consistent with this, the slope for extrasynaptic kalirin-7 was significantly greater than that of synaptic kalirin-7 ($F(1, 1340)=99.36$, $p<0.0001$; Fig. 2f), and the correlation coefficient for extrasynaptic kalirin-7 was almost identical to that of total kalirin-7 ($r^2=0.248$ for total kalirin-7). Overall, this indicates that extrasynaptic kalirin-7 is the primary contributor to the increase in net spine kalirin-7 content with increases in spine PSD area.

It is possible that the positive correlation between PSD area and extrasynaptic kalirin-7 particle number is due to a small proportion of large spines possessing an abnormally large

number of extrasynaptic particles. Conversely, it is possible that extrasynaptic kalirin-7 levels increase incrementally with corresponding incremental increases in PSD area. To investigate these possibilities, we binned PSD area and examined the mean kalirin-7 extrasynaptic particle number for each bin (Fig. 2g), and we also binned extrasynaptic kalirin-7 particle number and examined the corresponding mean PSD area (Fig. 2h). Overall, this analysis revealed gradual increases in extrasynaptic kalirin-7 particle number with increasing PSD area, and vice versa, supporting the idea that extrasynaptic kalirin-7 levels increase incrementally with increasing PSD area.

Axospinous synapses can be classified as perforated and non-perforated based on the morphology of the PSD. Perforated PSDs, which are typically larger and contain a greater number and concentration of AMPAR than non-perforated spines (Nicholson & Geinisman 2009), have a discontinuity in their PSD in at least one profile in serial sections. Non-perforated PSDs, a significant population of which lack AMPARs (Ganeshina *et al.* 2004; Nicholson & Geinisman 2009), have a continuous PSD in all serial sections (Nicholson et al. 2004). We compared kalirin-7 immunolabeling levels for spines with perforated or non-perforated PSDs (Fig. 3a-c). We first confirmed that perforated PSDs are larger than non-perforated PSDs ($p<0.0001$; Fig. 3d). Among synapses, 61% of non-perforated ones were immunonegative for kalirin-7 in synaptic compartments and 62% were immunonegative in extrasynaptic compartments. Approximately 55% of perforated synapses were immunonegative in the synaptic compartment, but only 25% were immunonegative in the extrasynaptic compartment. Despite their size difference, synaptic kalirin-7 particle number did not differ between perforated and non-perforated synapses ($p>0.05$; Fig. 3e), consistent with the observation that PSD area correlated only weakly with the amount of synaptically localized kalirin-7 (Figure 2f). Extrasynaptic kalirin-7 expression, however, was significantly greater among spines with perforated PSDs as compared to those bearing non-perforated PSDs ($p<0.001$; Fig. 3e). Within individual synapses, perforated ones have significantly more extrasynaptic kalirin-7 than synaptic kalirin-7 ($p<0.001$), whereas the level of immunoexpression among non-perforated synapses does not differ between the synaptic and extrasynaptic compartments ($p>0.05$; Fig. 3e). Thus, kalirin-7 expression has a specific relationship with PSD size, principally attributable to its increased prevalence extrasynaptically in large, mostly perforated, synapses.

The PSD analysis illustrates that there are at least two microdomains of kalirin-7 expression: one confined to the PSD and the other extended to the extrasynaptic milieu near the PSD. Perforated and non-perforated synapses differ in both PSD and spine size (Nicholson & Geinisman 2009), however, and consequently the PSD analysis may have underestimated extrasynaptic kalirin-7 immunoreactivity in both synapse subtypes, particularly in the smaller non-perforated ones. To address this notion directly, spines whose connection to their parent dendrite was visible in serial sections were identified, and then analyzed for kalirin-7 immunoexpression in the PSD, perisynaptically, and throughout the entire spine (Figure 4a, b). To assess whether or not there are more than two kalirin-7 microdomains, perisynaptic particles were considered those particles within a window that corresponds to the approximate depth of a typical PSD (20-60nm from the PSD). All other extrasynaptic particles were considered to be spinous.

Spine volume correlated strongly with PSD area for both perforated and non-perforated synapses ($r^2=0.861$; best fit slope=1.17±0.05; $p<0.0001$; Fig. 4c). Similar to what was found in the PSD analyses, there was a very weak relationship between spine volume and synaptic kalirin-7 immunoreactivity ($r^2=0.047$; best fit slope=12.85±5.80; $p<0.05$; Fig. 4d and g). Similarly, there was only a weak relationship between spine volume and perisynaptic kalirin-7 expression ($r^2=0.131$; best fit slope=25.30±6.52; $p<0.001$; Fig. 4e and g), and there was no difference in the slope for perisynaptic and synaptic kalirin-7 ($p>0.05$; Fig. 4g). The

relationship between spine volume and spinous kalirin-7, however, was very strong for spines bearing either synapse subtype (r^2=0.556; best fit slope=126.80±11.33; p<0.0001; Fig. 4f and g). Spinous kalirin-7 accounted for the vast majority of the relationship between total kalirin-7 immunoexpression and spine volume in both perforated an non-perforated synapses, as the slope for total kalirin-7 did not differ from that of spinous kalirin-7 for either synapse type (p>0.05), while the slope for spinous kalirin-7 was greater than that of synaptic and perisynaptic kalirin-7 (p<0.0001; Fig. 4g). Thus, this more comprehensive analysis supports the PSD analysis in identifying multiple kalirin-7 microdomains. Moreover, because of the strong correlation between PSD size and spine volume, this analysis complements and extends the PSD analysis and indicates that with regard to kalirin-7's expression profile, the extrasynaptic spinous domain is different from both the synaptic and perisynaptic domains.

Discussion

Taken together, our studies found that synapse size and spine volume were the principal components driving the localization of kalirin-7 within individual spines. Paradoxically, extrasynaptic rather than synaptic kalirin-7 localization varied most directly with size, such that spines with large PSDs had higher extrasynaptic kalirin-7 expression than those with small PSDs. It is important to note that synaptic kalirin-7 expression varied only weakly with synapse and spine size. Furthermore, with regard to kalirin-7 localization, the major difference between perforated and non-perforated spines lied in the localization of extrasynaptic kalirin-7, as synaptic kalirin-7 levels did not differ between these spine classes. The complete spine analysis found that extrasynaptic kalirin-7 expression is not necessarily confined to a perisynaptic annulus, but is rather more like a diffuse network of pools of kalirin-7 expression throughout the entire spine.

This is the first study to compare the location of an individual RacGEF as a function of spine morphology, and our findings indicate that extrasynaptic levels of kalirin-7 vary most directly with the size of individual spines and their synapses. Kalirin-7 is localized to the spine PSD via its interaction with numerous PDZ-domain containing scaffolding molecules, including PSD-95 and AF6, among others (Penzes et al. 2001b). Much less is known about the molecular mechanisms that stabilize kalirin-7 outside the spine PSD. Of potential importance is kalirin-7's ability to directly interact with the scaffolding molecule X11α (mLin-10, mint-1) (Penzes et al. 2001b). X11α is enriched in spines, yet shows a predominant localization extrasynaptically (Stricker & Huganir 2003), providing a potential means through which the stabilization of extrasynaptic kalirin-7 occurs.

The comparative functions of synaptic vs. extrasynaptic kalirin-7 merit future investigation. Insight into this problem comes from a recent study showing that the pool of actin required for long-term spine stabilization as seen in spines with large heads (the so-called stable pool of actin), is localized outside of the spine PSD (Honkura et al. 2008). Moreover, while the PSD itself contains a low concentration of actin molecules, extrasynaptic regions have an abundance of polymerized actin foci (Frost et al. 2010b). This suggests that molecules important for long-term spine stabilization, such as kalirin-7, might be strategically localized in the vicinity of the stable pool of actin throughout each spine.

Previous studies have indicated that within spines, actin-binding proteins are enriched outside the PSD (Racz & Weinberg 2008; Racz & Weinberg 2004). Given that the PSD largely lacks polymerized actin (Frost et al. 2010b), the localization of actin-binding proteins away from the PSD likely places them within the vicinity of F-actin. Within spines, GEFs directly interact with surface receptors in the PSD and relay signals to the actin cytoskeleton via a series of intermediary proteins, including actin-binding molecules (Penzes

& Jones 2008). That a RacGEF can show a prominent localization extrasynaptically within spines is surprising, and indicates that molecules acting well upstream of actin are not solely associated with the spine PSD. Our findings suggest that extrasynaptic kalirin-7 is an optimal position to regulate actin in spines and hence contribute to synapse morphology.

Kalirin-7's activity is inhibited by its interaction with scaffolding molecules enriched in the PSD (Penzes et al. 2001b), and recent studies have shown that synaptic activation, as assessed by electroconvulsive shock treatment and by NMDA receptor activation, reduces the interaction of kalirin-7 with PSD scaffolds. This is believed to foster kalirin-7's activation of its downstream effectors (Hayashi-Takagi et al. 2010). Whether activity-mediated disassociation of kalirin-7 from PSD scaffolds causes the extrasynaptic accumulation of kalirin-7 seen in large spines is unknown. Nevertheless, it supports the idea that the localization of kalirin-7 to spine domains outside the PSD is likely a significant contributor to the regulation of spine morphology. It is conceivable that synaptic and extrasynaptic kalirin-7 have differing roles in contributing to spine morphogenesis, such that in spines with small heads, synaptically localized kalirin-7 is in close proximity to synaptic signaling networks prominent in the PSD, which could prime kalirin-7 for activation once the proper signaling conditions are achieved. In large spines, the localization of kalirin-7 to perisynaptic regions would place kalirin-7 in closer proximity to the polymerized actin foci that ultimately dictate spine morphology.

Taken together, our findings indicate that an important molecule that relays signals from receptors to actin is subcompartmentalized in spines, and paradoxically, its extrasynaptic rather than its synaptic localization is most directly related to spine and synapse size.

Acknowledgments

This work was supported by grants from NIH-NIMH (R01MH071316) to P.P., NIH grants AG017139, AG031574, and AG020506 to D.A.N. and Y.G., and a Ruth L. Kirschstein National Research Service Award 1F31AG031621-01A2 to M.E.C. The authors declare no conflicts of interest with regard to the work presented. All experiments involving animals were done according to the Institutional Animal Care and Use Committee of Northwestern University. D.A.N., M.E.C., and C.T.T. performed research and analyzed results. M.E.C., D.A.N., and P.P wrote the paper, and P.P and Y.G contributed resources and necessary to complete this work.

Abbreviations used

EM	(electron microscopy)
GEF	(guanine nucleotide exchange factor)
PSD	(postsynaptic density)

References

Alvarez VA, Sabatini BL. Anatomical and physiological plasticity of dendritic spines. Annu Rev Neurosci. 2007; 30:79–97. [PubMed: 17280523]

Cahill ME, Jones KA, Rafalovich I, Xie Z, Barros CS, Muller U, Penzes P. Control of interneuron dendritic growth through NRG1/erbB4-mediated kalirin-7 disinhibition. Mol Psychiatry. 2012; 17(1):99–107.

Comery TA, Stamoudis CX, Irwin SA, Greenough WT. Increased density of multiple-head dendritic spines on medium-sized spiny neurons of the striatum in rats reared in a complex environment. Neurobiol Learn Mem. 1996; 66:93–96. [PubMed: 8946401]

Frost NA, Kerr JM, Lu HE, Blanpied TA. A network of networks: cytoskeletal control of compartmentalized function within dendritic spines. Curr Opin Neurobiol. 2010a; 20:578–587. [PubMed: 20667710]

Frost NA, Shroff H, Kong H, Betzig E, Blanpied TA. Single-molecule discrimination of discrete perisynaptic and distributed sites of actin filament assembly within dendritic spines. Neuron. 2010b; 67:86–99. [PubMed: 20624594]

Ganeshina O, Berry RW, Petralia RS, Nicholson DA, Geinisman Y. Synapses with a segmented, completely partitioned postsynaptic density express more AMPA receptors than other axospinous synaptic junctions. Neuroscience. 2004; 125:615–623. [PubMed: 15099675]

Glantz LA, Lewis DA. Decreased dendritic spine density on prefrontal cortical pyramidal neurons in schizophrenia. Arch Gen Psychiatry. 2000; 57:65–73. [PubMed: 10632234]

Hayashi-Takagi A, Takaki M, Graziane N, et al. Disrupted-in-Schizophrenia 1 (DISC1) regulates spines of the glutamate synapse via Rac1. Nat Neurosci. 2010; 13:327–332. [PubMed: 20139976]

Honkura N, Matsuzaki M, Noguchi J, Ellis-Davies GC, Kasai H. The subspine organization of actin fibers regulates the structure and plasticity of dendritic spines. Neuron. 2008; 57:719–729. [PubMed: 18341992]

Jones KA, Srivastava DP, Allen JA, Strachan RT, Roth BL, Penzes P. Rapid modulation of spine morphology by the 5-HT2A serotonin receptor through kalirin-7 signaling. Proc Natl Acad Sci U S A. 2009; 106:19575–19580. [PubMed: 19889983]

Ma XM, Johnson RC, Mains RE, Eipper BA. Expression of kalirin, a neuronal GDP/GTP exchange factor of the trio family, in the central nervous system of the adult rat. J Comp Neurol. 2001; 429:388–402. [PubMed: 11116227]

Newpher TM, Ehlers MD. Spine microdomains for postsynaptic signaling and plasticity. Trends Cell Biol. 2009; 19:218–227. [PubMed: 19328694]

Nicholson DA, Geinisman Y. Axospinous synaptic subtype-specific differences in structure, size, ionotropic receptor expression, and connectivity in apical dendritic regions of rat hippocampal CA1 pyramidal neurons. J Comp Neurol. 2009; 512:399–418. [PubMed: 19006199]

Nicholson DA, Trana R, Katz Y, Kath WL, Spruston N, Geinisman Y. Distance-dependent differences in synapse number and AMPA receptor expression in hippocampal CA1 pyramidal neurons. Neuron. 2006; 50:431–442. [PubMed: 16675397]

Nicholson DA, Yoshida R, Berry RW, Gallagher M, Geinisman Y. Reduction in size of perforated postsynaptic densities in hippocampal axospinous synapses and age-related spatial learning impairments. J Neurosci. 2004; 24:7648–7653. [PubMed: 15342731]

Penzes P, Cahill ME, Jones KA, Srivastava DP. Convergent CaMK and RacGEF signals control dendritic structure and function. Trends Cell Biol. 2008; 18:405–413. [PubMed: 18701290]

Penzes P, Cahill ME, Jones KA, VanLeeuwen JE, Woolfrey KM. Dendritic spine pathology in neuropsychiatric disorders. Nat Neurosci. 2011; 14:285–293. [PubMed: 21346746]

Penzes P, Johnson RC, Alam MR, Kambampati V, Mains RE, Eipper BA. An isoform of kalirin, a brain-specific GDP/GTP exchange factor, is enriched in the postsynaptic density fraction. J Biol Chem. 2000; 275:6395–6403. [PubMed: 10692441]

Penzes P, Johnson RC, Kambampati V, Mains RE, Eipper BA. Distinct roles for the two Rho GDP/GTP exchange factor domains of kalirin in regulation of neurite growth and neuronal morphology. J Neurosci. 2001a; 21:8426–8434. [PubMed: 11606631]

Penzes P, Johnson RC, Sattler R, Zhang X, Huganir RL, Kambampati V, Mains RE, Eipper BA. The neuronal Rho-GEF Kalirin-7 interacts with PDZ domain-containing proteins and regulates dendritic morphogenesis. Neuron. 2001b; 29:229–242. [PubMed: 11182094]

Penzes P, Jones KA. Dendritic spine dynamics--a key role for kalirin-7. Trends Neurosci. 2008; 31:419–427. [PubMed: 18597863]

Racz B, Weinberg RJ. The subcellular organization of cortactin in hippocampus. J Neurosci. 2004; 24:10310–10317. [PubMed: 15548644]

Racz B, Weinberg RJ. Organization of the Arp2/3 complex in hippocampal spines. J Neurosci. 2008; 28:5654–5659. [PubMed: 18509026]

Silva-Gomez AB, Rojas D, Juarez I, Flores G. Decreased dendritic spine density on prefrontal cortical and hippocampal pyramidal neurons in postweaning social isolation rats. Brain Res. 2003; 983:128–136. [PubMed: 12914973]

Stricker NL, Huganir RL. The PDZ domains of mLin-10 regulate its trans-Golgi network targeting and the surface expression of AMPA receptors. Neuropharmacology. 2003; 45:837–848. [PubMed: 14529721]

Xie Z, Srivastava DP, Photowala H, Kai L, Cahill ME, Woolfrey KM, Shum CY, Surmeier DJ, Penzes P. Kalirin-7 controls activity-dependent structural and functional plasticity of dendritic spines. Neuron. 2007; 56:640–656. [PubMed: 18031682]

Yuste R. Dendritic spines and distributed circuits. Neuron. 2011; 71:772–781. [PubMed: 21903072]

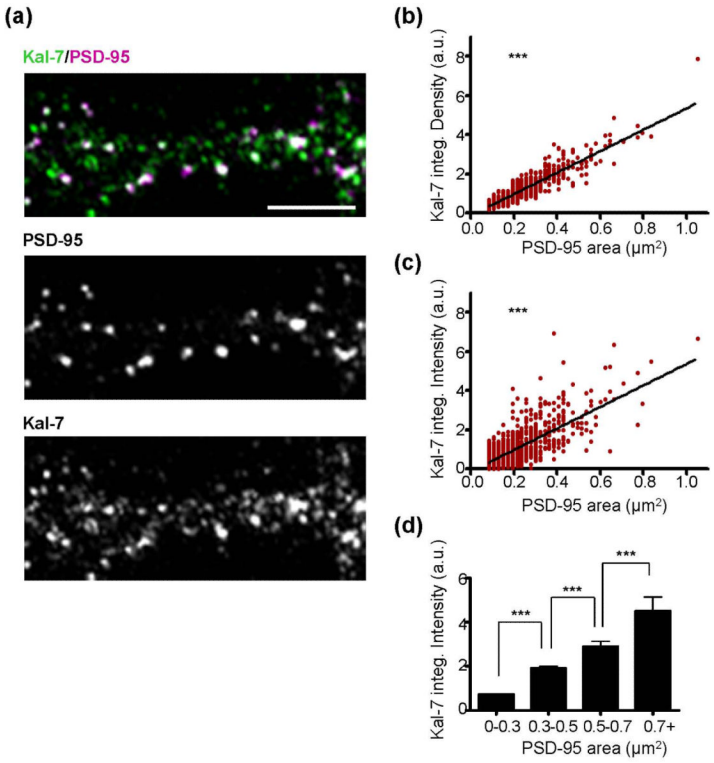

Fig. 1.

Relationship between PSD-95 area and kalirin-7 content. (a) DIV26 cultured cortical neurons were immunostained for endogenous kalirin-7 and endogenous PSD-95. The top image shows kalirin-7 and PSD-95 together; white color in top image occurs in areas of colocalization between kalirin-7 and PSD-95. Individual kalirin-7 and PSD-95 channels are shown in the lower images. Scale bars=5μm. (b) As PSD-95 puncta area increases, there is a corresponding increase in kalirin-7 integrated density (PSD-95 area x mean kalirin-7 fluorescent intensity; a.u., arbitrary units). Scatter plot with linear regression curve for all cells analyzed is shown; each point represents a single psd-95 puncta. N=1105 puncta from 8 cells and significance determined using linear regression and the deviation from a slope of 0. ***$p<0.0001$. (c) Analysis as in (b) showing kalirin-7 integrated intensity (sum of kalirin-7 fluorescent intensity within PSD-95 area; a.u., arbitrary units). Significance determined using linear regression and the deviation from a slope of 0. ***$p<0.0001$. (d) Graph shows binned PSD-95 area with the corresponding mean kalirin-7 integrated intensity. N=1105 puncta from 8 cells and significance determined using a one-way ANOVA with Tukey post-hoc test. Data are the mean±SEM. ***$p<0.001$.

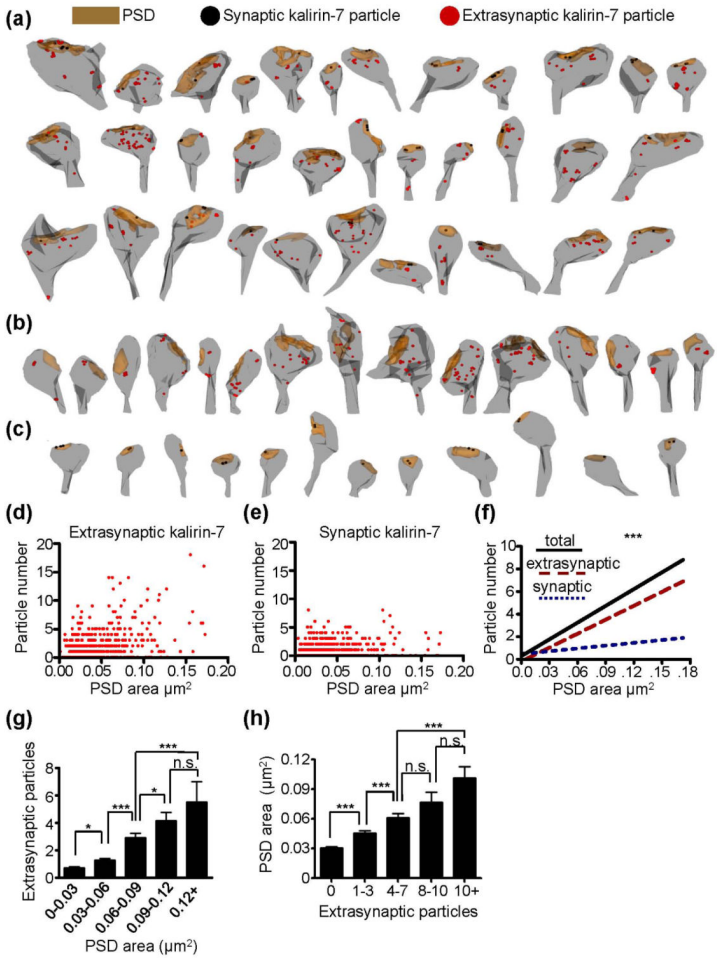

Fig. 2.

Ultrastructural localization of kalirin-7 within spines. (a-c) Immuno-EM reconstructions showing the postsynaptic density (brown), single synaptic (black circles) and single extrasynaptic (red circles) particles for kalirin-7 puncta. The three major phenotypes for kalirin-7 immunoreactive spines were those with both synaptic and extrasynaptic expression (a), those with only extrasynaptic expression (b), and those with only synaptic expression (c). (d) Scatterplot showing PSD area and the number of extrasynaptic kalirin-7 particles for individual perforated synapses. Each point represents a single synapse. (e) Scatterplot showing PSD area and the number of synaptic kalirin-7 particles for individual perforated synapses. Each point represents a single synapse. (f) Linear regression curves for total, synaptic, and extrasynaptic kalirin-7 particle number per synapse as a function of PSD area. The slope for perisynaptic kalirin-7 is significantly greater than the slope for synaptic kalirin-7 (***). N=672 synapses. Significant differences between slopes determined using linear regression analysis. ***p<0.0001. (g) Binned PSD areas of synapses are shown with the corresponding mean extrasynaptic kalirin-7 particle number. Significance determined using a one-way ANOVA with Tukey post-hoc test. Data are the mean±SEM. *p<0.05, ***p<0.001, n.s. not significant. (h) Binned extrasynaptic kalirin-7 particle numbers are shown with the corresponding mean PSD area. Significance determined using a one-way ANOVA with Tukey post-hoc test. Data are the mean±SEM. ***p<0.001, n.s. not significant.

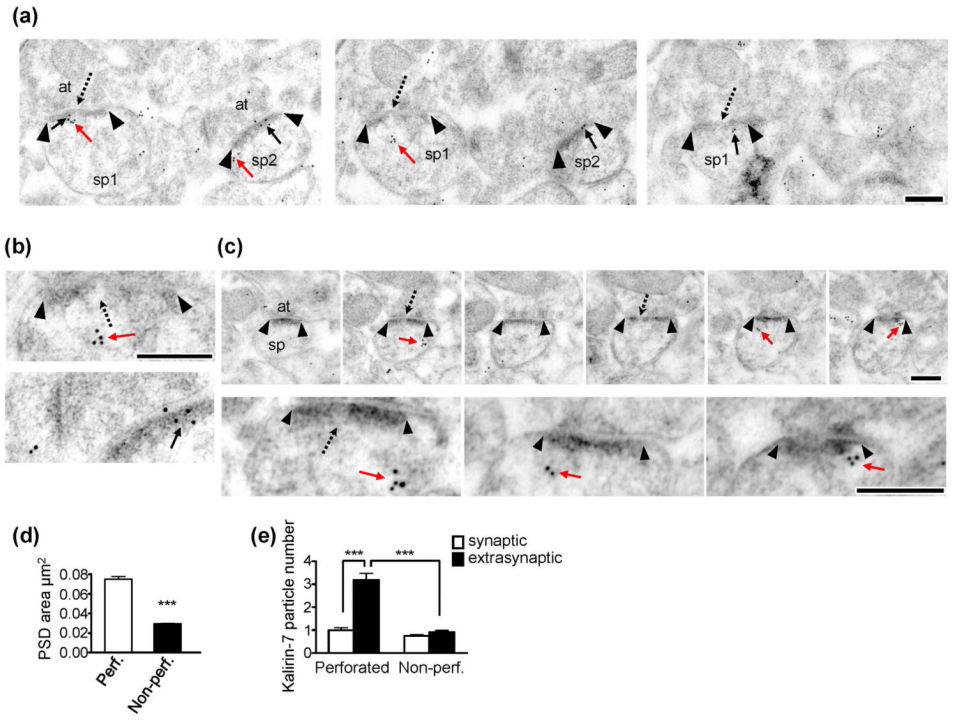

Figure. 3.

Ultrastructural localization of kalirin-7 in perforated and non-perforated synapses. (a) Immuno-EM images from serial sections showing kalirin-7 particle localization relative to the PSD for non-perforated and perforated synapses. Black arrowheads denote the borders of the PSD. Solid black arrows show synaptic kalirin-7 particles; solid red arrows show extrasynaptic particles for kalirin-7. Dashed black arrows point to the perforations or discontinuities in the PSD. sp1 = spine 1 (perforated); sp2 = spine 2 (non-perforated); at=axon terminal. Scale bars = 250nm. (b) High magnification images. Top, a perforated spine with kalirin-7 particles located outside of the PSD. Bottom, a non-perforated spine in which all kalirin-7 particles are located within the PSD. Scale bar = 250nm. (c) Serial sections through a perforated synapse showing significant levels of extrasynaptic kalirin-7. Upper images show low magnification while lower images show higher magnification of the same spine. Black arrowheads show the borders of the postsynaptic density. Solid red arrows show extrasynaptically localized kalirin-7 puncta. Dashed black arrows indicate perforations or discontinuities in the postsynaptic density. sp=spine; at=axon terminal. Scale bar=250nm. (d) Bar graphs showing that perforated synapses are larger than non-perforated ones. N=506 non-perforated and 166 perforated synapses. Data are mean±SEM. ***p<0.0001. (e) Extrasynaptic and synaptic kalirin-7 particle number as a function of PSD configuration. In non-perforated synapses, kalirin-7 particle number was similar in the synaptic and extrasynaptic domains. Perforated synapses, on the other hand, had significantly greater levels of kalirin-7 expression in the extrasynaptic domains than synaptically (***), and had significantly more extrasynaptic kalirin-7 expression than non-perforated synapses (***). Data are mean±SEM. Significance determined using a 2×2 ANOVA with Bonferroni post-hoc test. ***p<0.001.

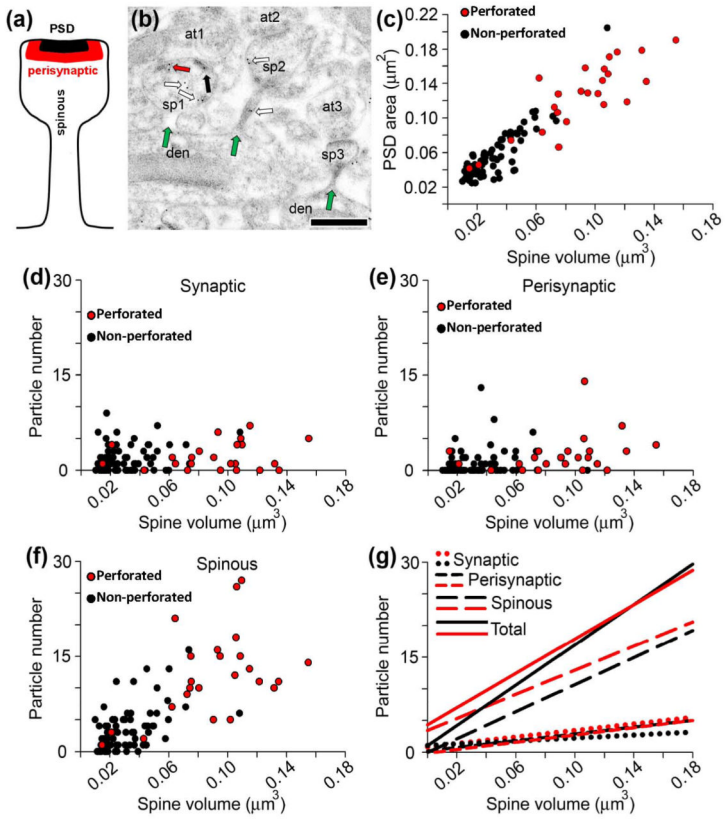

Figure 4.

Kalirin-7 expression in microdomains throughout entire spines. (a) Schematic depiction of a dendritic spine denoting the location of the three microdomains of kalirin-7 expression. (b) An electron micrograph showing three spines (sp1, sp2, and sp3) and their attachment to their parent dendrites (green arrows). As illustrated in this figure, throughout the whole population of spines and synapses, synaptic (black arrows), perisynaptic (red arrows), and spinous (white arrows) kalirin-7 particles are seen in some spines but not others, Scale bar = 500 nm, (c) Scatterplot showing that spine volume correlates closely with PSD area in both perforated (red) and non-perforated (black) synapses. N = 24 spines with a perforated synapse; N = 78 spines with a non-perforated synapse. (d) Scatterplot showing only a weak relationship between spine volume and synaptic kalirin-7 expression. (e) Scatterplot showing only a weak relationship between spine volume and perisynaptic kalirin-7 expression. (f) Scatterplot showing the strong relationship between non-synaptic spinous kalirin-7 expression and spine volume. (g) Linear regression curves for total, synaptic, perisynaptic, and extrasynaptic kalirin-7 particle number per spine as a function of spine volume. Spinous kalirin-7 expression accounts for the majority of the relationship between spine volume and total kalirin-7 particle numbers.